Physiological changes may dominate the electrical properties of liver during reversible electroporation: Measurements and modelling

Tomas Garcia-Sanchez, Damien Voyer, Clair Poignard, Lluis M. Mir

▶ **To cite this version:**

Tomas Garcia-Sanchez, Damien Voyer, Clair Poignard, Lluis M. Mir. Physiological changes may dominate the electrical properties of liver during reversible electroporation: Measurements and modelling. Bioelectrochemistry, 2020, 136, pp.107627. 10.1016/j.bioelechem.2020.107627 . hal-02914095

HAL Id: hal-02914095
https://inria.hal.science/hal-02914095

Submitted on 11 Aug 2020

HAL is a multi-disciplinary open access archive for the deposit and dissemination of scientific research documents, whether they are published or not. The documents may come from teaching and research institutions in France or abroad, or from public or private research centers.

L'archive ouverte pluridisciplinaire **HAL**, est destinée au dépôt et à la diffusion de documents scientifiques de niveau recherche, publiés ou non, émanant des établissements d'enseignement et de recherche français ou étrangers, des laboratoires publics ou privés.

Bioelectrochemistry 136 (2020) 107627

Contents lists available at ScienceDirect

Bioelectrochemistry

journal homepage: www.elsevier.com/locate/bioelechem

Physiological changes may dominate the electrical properties of liver during reversible electroporation: Measurements and modelling

Tomás García-Sánchez [a,b,*,1], Damien Voyer [c,d,1], Clair Poignard [d], Lluis M. Mir [a]

[a] Université Paris-Saclay, Institut Gustave Roussy, CNRS, Metabolic and Systemic Aspects of Oncogenesis (METSY), 94805 Villejuif, France
[b] Department of Information and Communication Technologies, Universitat Pompeu Fabra, Barcelona, Spain
[c] EIGSI La Rochelle, La Rochelle Cedex F-17041, France
[d] Team MONC, INRIA, CNRS UMR 5251, Bordeaux INP, Talence Cedex F-33405, France

ARTICLE INFO

Article history:
Received 7 May 2020
Received in revised form 30 July 2020
Accepted 30 July 2020
Available online 1 August 2020

ABSTRACT

This study presents electrical measurements (both conductivity during the pulses and impedance spectroscopy before and after) performed in liver tissue of mice during electroporation with classical electrochemotherapy conditions (8 pulses of 100 μs duration). A four-needle electrode arrangement inserted in the tissue was used for the measurements. The undesirable effects of the four-electrode geometry, notably concerning its sensitivity, were quantified and discussed showing how the electrode geometry chosen for the measurements can impact the results. Numerical modelling was applied to the information collected during the pulse, and to the impedance spectra acquired before and after the pulses sequence. Our results show that the numerical results were not consistent, suggesting that other collateral phenomena not considered in the model are at work during electroporation in vivo. We show how the modification in the volume of the intra and extra cellular media, likely caused by the vascular lock effect, could at least partially explain the recorded impedance evolution. In the present study we demonstrate the significant impact that physiological effects have on impedance changes following electroporation at the tissue scale and the potential need of introducing them into the numerical models. The code for the numerical model is publicly available at https://gitlab.inria.fr/poignard/4-electrode-system.
© 2020 Elsevier B.V. All rights reserved.

1. Introduction

The measurement of the electrical properties of cells and tissues has been commonly used as simple and reliable label-free method to assess electroporation. The state of increased membrane permeability to molecular species caused by a short-duration, high-intensity electric field exposure that represents the basis of the electroporation phenomenon has direct consequences in the electrical conductivity of the exposed sample. Namely, an immediate and abrupt increase in electrical conductivity is detected as a result of membrane pore opening during the pulse application. Early studies already used conductivity measurements to perform a comprehensive characterization of electropermeabilization [1]. Since then, many studies have used electrical measurements to characterize, predict or assess electroporation from different perspectives. In fundamental studies, electrical measurements could reveal the pore dynamics (formation, expansion, shrinkage) [2]. On the other hand, there is an ongoing technological research to develop electrical measurement tools to provide real-time feedback control systems for treatments based on electroporation, for instance to prevent, or optimize irreversible electroporation (IRE) [3–6].

The changes in the electrical properties of cells (in vitro or in living tissues) can be studied during pulse application by calculating the ratio between the recorded voltage and current waveforms. This quasi-DC resistance information displays a dynamic behavior during pulse duration (usually 100 μs) with an abrupt increase of conductivity followed by a slower exponential increase during the rest of the pulse. Because electroporation protocols always include sequences of multiple pulses aiming to produce a cumulative effect, conductivity measurements should also reflect this accumulated effect pulse after pulse. However, controversial results have been reported in the literature in this respect. Particularly, in the case of living tissues, repetitive pulses not always display the expected conductivity increase pulse after pulse, or only during the first few pulses followed by a saturation effect depending on the pulsing conditions [7–9]. However, results from in vitro studies using similar pulsing conditions to the previously mentioned in vivo results (sequences of 100 μs pulses at 1 Hz repetition

* Corresponding author.
E-mail address: tomas.garcia@upf.edu (T. García-Sánchez).
[1] Both authors contributed equally to this work.

https://doi.org/10.1016/j.bioelechem.2020.107627
1567-5394/© 2020 Elsevier B.V. All rights reserved.

frequency) demonstrate that the level of permeabilization continues increasing during the whole pulse sequence [10,11].

Electrical properties have also been assessed after electroporation pulses mostly by measuring the complex impedance changes. In this type of measurements, the impedance at multiple frequencies is usually assessed by applying a low amplitude signal (impedance spectroscopy). Previous studies in vivo suggested that this type of measurements could reflect the treatment outcome in a more accurate way compared to in-pulse measurements [12]. Both in vitro and in vivo, bioimpedance measurements have shown their potential for monitoring cell resealing after pulses. However, a clear drawback of these measurements is their low specificity, meaning that different phenomena could produce the observed impedance changes [13]. Special care should be taken in the case of living tissues where a combination of the effects directly related to membrane poration maybe be mixed with other physiological changes that take place also after the pulses but with opposite trends [14].

Another aspect that must be considered when performing electrical measurements during electroporation and that introduces uncertainties in the measurements is the electrode interference. Most of the studies in the literature have used the same pair of electroporation electrodes to acquire voltage and current in conductivity (or impedance) recordings. However, this 2-electrode approach maybe highly impacted by the impedance present at the interface electrode/electrolyte. For the in-pulse conductivity measurements, the high intensity pulses that are applied to electrodes produce a non-linear decrease of this electrode/electrolyte impedance [15] that could theoretically make its contribution negligible, however, no experimental study has been performed to confirm that. On the opposite, some studies have shown that other changes in the electrodes are produced during pulse application [16] with a possible impact on measurements. In the case of complex impedance measurements, where a small signal is applied to the electrodes, interfacial water near the electrodes may have a strong impact especially at low frequencies. One common approach to avoid this low frequency interfacial distortion is to use a 4-electrode arrangement where an additional pair of electrodes connected to a high input impedance system is used to measure the voltage [17,18]. In the field of electroporation, only few studies have used 4-electrode arrangements to measure impedance [12,19].

In this context, numerical modeling appears to be a powerful tool to facilitate the understanding of the data both concerning the resistance measured during the pulse and the impedance spectra recorded after the pulse. The models to describe the electric response during the pulse are all based on the non-linear electrokinetic equations where the electrical properties of tissues are described in a more or less complex way. One of the most popular approaches is to model the tissue as a material whose conductivity varies non-linearly according to the electric field [7,20]. Recently, more sophisticated models have been introduced to describe the dynamic evolution of conductivity during the pulse; for example, the model proposed in [21] at the tissue scale introduces the contribution of each compartment (intra and extra cellular media, membrane) and establishes the link with the models developed at the cell scale. These models most often make it possible to reproduce the measurements carried out, in particular because they take into account the real geometry of the electrodes that has a crucial effect on the distribution of the electric field. On the other hand, it is difficult to estimate properly the parameters of the model: very often, the simulations are carried out using the data reported in the literature that provide ranges of values because of the variability in biological tissues.

Furthermore, spectroscopy measurements are always analyzed using equivalent electrical circuits to describe the frequency behavior of the tissue sample under test. The most popular model is based on a physical interpretation [22,23] where a Constant Phase Element (CPE) element is introduced to describe the dispersion observed in the impedance spectrum; an alternative model, more compact, is based on a mathematical approach using Cole equation [8].

To our knowledge, there is no study where the information collected during the pulse and the impedance spectrum performed before and after the pulse are correlated in the same experiment in order to check the consistency of the simulation results provided by the numerical modeling. However, such an approach would be instructive as electrical measurements can be affected by many physical and physiological phenomena as mentioned previously. Except the influence of the temperature which is naturally introduced in electroporation applications, other phenomena such as the change of intra and extra cellular volumes or the change of ionic concentrations are generally not taken into account in electrical simulations at the tissue scale.

The present study deals with electrical measurements (both in pulse conductivity and impedance spectroscopy data) performed in liver tissue of mice during in vivo electroporation. For the first time, a four-needle electrode arrangement directly inserted in the tissue is used for this type of measurements. Numerical modelling is applied to the data in an attempt to make a correct interpretation of the data recorded during and after the application of the pulses. The undesirable effects of the four-electrode system, notably concerning its sensitivity, are quantified and discussed. Finally, it appears that the consistency of the numerical modeling is questionable: physiological effects induced inside the tissue by the application of electroporation are highlighted and their effects on the electrical properties of the tissue are discussed.

2. Materials and methods

2.1. Measurement setup

Electrical measurements of the liver tissue before, during and after electroporation pulses were acquired using a four-electrode setup composed by two pairs of stainless steel needles. The dimensions of the actual needle arrangement are shown in Fig. 1. The external pair of needles (diameter = 0.45 mm) was used to apply the electroporation pulses to the tissue and for current recordings while the internal pair of needles (diameter = 0.25 mm) was used to record the voltage. All the measured impedances discussed in this work are defined as the ratio of the voltage between the internal needles to the current flowing in the external needles.

The four electrode topology was used to avoid any possible artifact in the voltage measurements introduced by the interfacial electrode polarization. As the internal pair of needles used for voltage measurements are connected to a high input impedance differential amplifier, the theoretical current passing through these electrodes is negligible. Therefore, the voltage measurement is not affected by the voltage drop due to the impedance that generally appears at the interface between the electrodes and the tissue. From a modeling point of view, it is then not necessary to model this impedance and this is very interesting since the modeling might involve non-linear effects [24] because of the amplitude of the electric field applied in the electroporation process. Contrarily to the measurements usually performed with only two electrodes, which sense the voltage at the generator output and do not take into account the possible voltage drop in the application electrodes, this strategy allowed us to measure the actual voltage that drops only in the tissue.

Electroporation pulses were generated by an electroporation power supply (CliniporatorTM, Igea, Carpi, Italy). In this study,

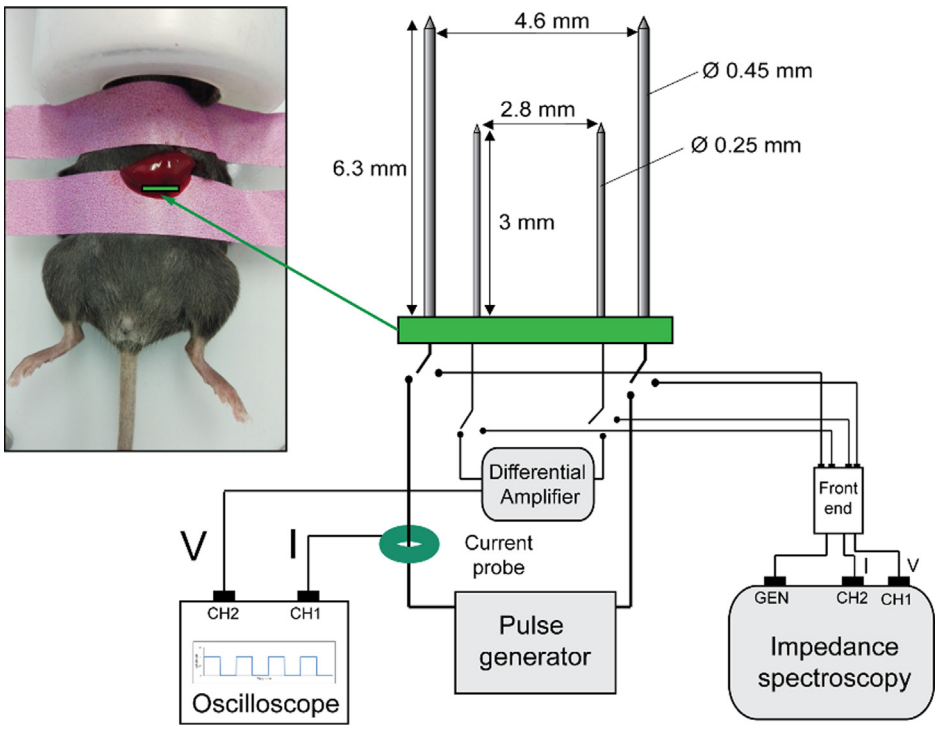

Fig. 1. Experimental setup for the electrical measurements using a four-electrode arrangement.

the classical sequence of 8 square, monopolar pulses of 100 μs duration applied at a repetition rate of 1 Hz was used. The effects at different pulse amplitudes were studied.

2.1.1. Voltage/current in pulse measurements

In order to measure the intra-pulse conductivity changes during electroporation pulses application, the voltage across the internal electrodes was measured with an active high-voltage differential probe (model TA042, Pico Technologies), the current flowing through the external needles was measured using a clamp-on current probe (model TCP2020, Tektronix). Both probes were connected to a digital oscilloscope (WaveMaster 808Zi, Lecroy) whose memory was segmented to acquire current and voltage measurements only during the electroporation pulses with a high temporal resolution (10 MS/s).

In order to acquire a reference measurement before the electroporation pulses, 2 low-voltage pulses (average electric field at the center of the domain <150 V/cm) were applied with the same electroporation power supply immediately before the electroporation pulses.

The instantaneous resistance values (refer to Section 3.1.2) were calculated by averaging the voltage and current ratio over the last 8 μs of the 100 μs pulses. Before electroporation, the values correspond to the average of the 2 low-voltage pulses; during electroporation, values are the mean of the 8 pulses sequence (this last calculation was possible because we did not observe an evolution of the values over the 8 pulses sequence).

2.1.2. Electrical impedance spectroscopy measurements

In a different set of experiments, complex impedance spectra were acquired before and after electroporation using the same four-needle topology previously described. Electrodes were manually switched between the electroporation generator and a custom-made impedance spectroscopy measuring system based on a PXI platform (National Instruments). This measuring setup comprised an arbitrary waveform generator (NI-PXI 5422) that injects multisine excitations (each multisine burst contained 26 frequencies distributed from 1 kHz to 1 MHz with a duration of 1 ms, current intensity <1 mA) and records voltage and current with a two channels digitizer (NI-PXIe 5122), from which complex impedance was calculated. Additionally, a custom-made analog front-end was used to interface the measuring signals with the electrodes. More details about a very similar setup can be found in [25].

Impedance measurements were acquired every second, and each measurement point was calculated from the average of 100 spectra acquired continuously (100 ms). The sequence started with 10 measurements performed before electroporation pulses; immediately after the pulses, impedance spectra were acquired during 10 min, which corresponds to 600 measurements.

2.2. Animals and anesthesia

The left liver lobe from 5 to 7 week-old female and male SV129 mice was used as target tissue for this study. Animals were first anesthetized with 2% isoflurane/oxygen mixture gas anesthesia in an induction chamber; gas anesthesia was maintained with a mask during the whole procedure until euthanasia. A small incision on the left subcostal region was performed to expose the left liver lobe. Needle electrodes were then inserted parallel to the horizontal plane and fixed, excess bleeding was dried out before starting the measurement-electroporation sequence. All animals were euthanized at the end of the procedure.

Animals were housed and handled according to recommended guidelines (UKCCCR). All the procedures described were approved by the French Ministry of research after ethical evaluation by the CEEA 26 committee (project number 2018_014_13409).

2.3. Mathematical models

2.3.1. Equivalent circuit model

In order to interpret the impedance measurements, a classical circuit model [20,28] can be used to describe the tissue (see Fig. 2). This model is composed of four elements: a resistance R_{ext}

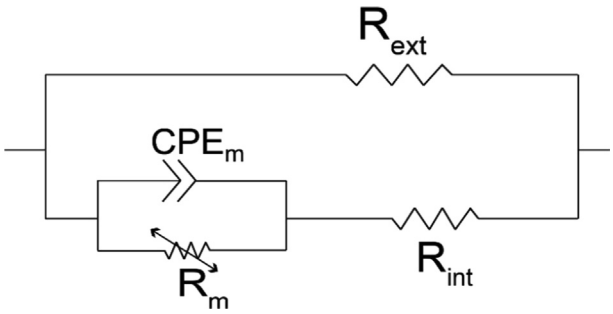

Fig. 2. Complete electrical model for the tissue.

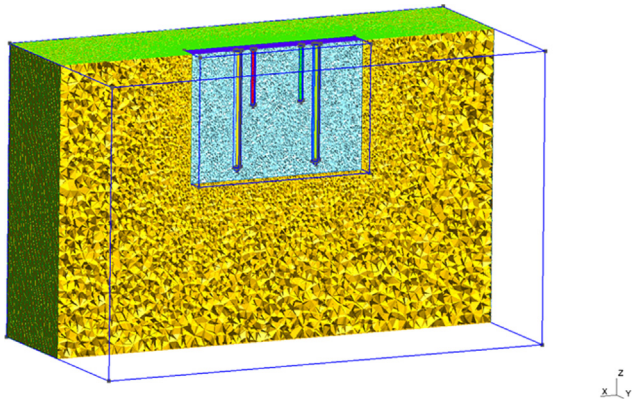

Fig. 3. 3D mesh of the 4-electrode finite element model.

for the contribution of the extra cellular medium, a resistance R_{int} for the contribution of the intra cellular medium, a Constant Phase Element (CPE) $Z_{CPE} = 1/\beta \times (j\omega)^{\alpha}$ for the pseudo-capacitive contribution of the membranes and a resistance R_m in parallel to the CPE that is introduced to better model the process of electroporation. More precisely, the CPE models the relaxation of the interfacial polarization that appears between the cell membranes and the intra or extra cellular media; the parameter α is necessary in order to model the distribution of the different time constants present in a living tissue [29]. Moreover, the resistance R_m is very high in normal conditions but should importantly drop due to the increase in the permeability of the cell membranes during electroporation.

During the pulse, a high voltage v(t) is applied between the external electrodes. The current i(t) that flows through these electrodes as well as the voltage u(t) induced between the internal electrodes are measured at the same time: in those conditions, the instantaneous resistance can be computed as $R_{pulse}(t) = u(t)/i(t)$. We will focus our attention at the end of the pulses where a quasi-DC regime is reached as it will be shown in Section 3.1.2.

From a theoretical point of view, only the conductive part of the tissue affects the measured impedance in the static regime ($\omega \to 0$). In the model of Fig. 2, the CPE is open circuit ($Z_{CPE} \to \infty$) and the current flows only through the resistances of the model.

In view of the above considerations, the equivalent circuit at the end of the pulse is given by a resistance R_{ext} in parallel with a branch composed of two resistances R_{int} and R_m in series. Then, the equivalent resistance of the tissue in the quasi DC regime verifies:

$$\frac{1}{R_{eq}} = \frac{1}{R_{int} + R_m} + \frac{1}{R_{ext}} \tag{1}$$

2.3.2. Finite element model

In order to predict the spatial distribution of electroporated tissue, we built a 3D model of the 4-electrode device presented in Fig. 1 using the open source mesh generator Gmsh [28] (see Fig. 3).

The distribution of the electric potential φ in the resulting geometry was computed solving a nonlinear electrokinetics equation where the tissue conductivity σ_{eq} depends on the magnitude of the electric field E [7,29]:

$$\nabla \cdot (\sigma_{eq}(E)\nabla\varphi) = 0 \tag{2}$$

where $E = |\nabla\varphi|$

The numerical problem was formulated using the finite element method and the nonlinear solution was computed with an iterative method [26] using the open source software Freefem++ [27] (see Supplementary Information II).

2.3.2.1. Tissue conductivity model. The model that sets the relationship between the tissue conductivity and the magnitude of the electric field is derived from a static model of electroporation provided in literature [7] and from the tissue characteristics measured before electroporation. It is worth noting that this model is consistent with the circuit model described in the Section 2.1.1. Introducing a form factor K that quantifies the ratio between the global resistance R measured by the four electrodes system and the resistivity $1/\sigma$ of the sample under test ($R = K/\sigma$), Eq. (1) can be expressed in terms of equivalent conductivity as follows:

$$\sigma_{eq} = \frac{\sigma_{int}\sigma_m}{\sigma_{int} + \sigma_m} + \sigma_{ext} = \frac{\sigma_{int}}{1 + \sigma_{int}/\sigma_m} + \sigma_{ext} \tag{3}$$

where σ_{eq}, σ_{ext}, σ_{int} and σ_m are the equivalent conductivities of the extracellular medium, the intracellular medium and the cell membranes, respectively.

Before the electroporation process begins, $\sigma_m \to 0$ and the equivalent conductivity of the tissue reaches its lower value $\min(\sigma_{eq}) = \sigma_{ext}$. When the membrane is fully permeabilized, it is generally assumed that $\sigma_m \gg \sigma_{int}$ and the equivalent conductivity of the tissue reaches then its larger value $\max(\sigma_{eq}) = \sigma_{ext} + \sigma_{int}$. Between those extremes values, the evolution of the equivalent conductivity given in Eq. (3) can be modeled with a sigmoid function with respect to the electric field intensity [7]:

$$\sigma_{eq}(E) = \frac{\sigma_{int}}{1 + exp\left(-\frac{E-a}{b}\right)} + \sigma_{ext} \tag{4}$$

where {a, b} are the parameters of the sigmoid function. σ_{ext} and σ_{int} have been set using experimental data (see Supplementary Information I, part A) while {a = 650 V/cm, b = 30 V/cm} have been chosen with respect to the values found in literature for a liver tissue [7].

It is worth noting that the sigmoid function in Eq. (4) is chosen empirically. There are other nonlinear conductivity models that could fit the experimental data. In this paper, we tested another nonlinear model of the conductivity based on the following sigmoid function:

$$\sigma_{eq}(E) = \frac{\sigma_{int}}{1 + exp\left(\frac{a'^2}{E^2}\right)} + \sigma_{ext} \tag{5}$$

where a' is the parameter of the sigmoid function. The sigmoid function in Eq. (5) involves the ratio of electrical energies: it is somehow the tissue version of the Krassowska et al model for cell electroporation, which involved the ratio $(V_m/V_{ep})^2$ where V_m is the transmembrane potential and V_{ep} the characteristic electroporation voltage (see Eq. (3) in [34]). The analysis of both sigmoid functions in Eqs. (4) and (5) with regard to Eq. (3) show that in both

cases, $\sigma_m \ll \sigma_{int}$ when the electric field is much lower than the electroporation threshold. But when the tissue is fully electroporated, the sigmoid function in Eq. (4) implies that $\sigma_m \gg \sigma_{int}$ while the sigmoid function in Eq. (5) suggests that σ_m is at best order of σ_{int}.

In addition, to refine the model provided by Eq. (4) or (5), the effect of the temperature increase during the pulse may be taken into account introducing a correction term [32,33]. In the case of the model provided by Eq. (4), the modified conductivity reads:

$$\sigma_{eq}(E,\Delta T) = \left[\frac{\sigma_{int}}{1+exp\left(-\frac{E-a}{b}\right)} + \sigma_{ext}\right] \times (1+\alpha_T \Delta T) \quad (6)$$

where the increase of temperature ΔT is computed from the Joule heating without considering thermal diffusion, blood flow, metabolic heat and electrode heat dissipation [32]:

$$\Delta T = \frac{\sigma_{eq} E^2}{\rho c_p} \Delta t \quad (7)$$

where ρ is the tissue density, c_p the tissue heat capacity and Δt the cumulated duration of the applied voltage for the sequence of 8 pulses.

2.3.2.2. Impedance computation and sensitivity. The numerical solution provides the distribution of the electric field expected in the static case: we did not take into account the capacitive effects nor the dynamics of the electroporation process which play a role mainly at the beginning of the pulse. Thus, the resistance R_{eq} we calculated is only valid at the end of the pulse. To avoid mesh-related errors in the impedance computation, the current injected through the external electrodes was calculated from the power dissipated throughout the entire system (volume integral) and the voltage between the internal electrodes was determined directly by evaluating the value of the potential at the surface of the passive electrodes which are isopotential.

In an ideal system composed by two infinite parallel plates and neglecting any electrode polarization effect, the impedance evolution with respect to the applied voltage would perfectly follow the sigmoid function described in Eq. (4), (5) or (6). However, due to the four-electrode topology where a current is injected through the external needles and the voltage is measured between the internal needles, the inhomogeneous conductivity distribution may affect the impedance changes in a non-intuitive way. It is indeed important to consider how each local region contributes to the total calculated impedance. The sensitivity *S*, defined as the local contribution of each piece of tissue to the global impedance, can provide a quantification of this effect as follows [30]:

$$S = \frac{1}{\sigma} \vec{E}_1 \cdot \vec{E}_2 \quad (8)$$

where E_1 is the electric field induced when a current of 1A is injected in the external electrodes while the internal electrodes are passive; E_2 is the electric field induced when a current of 1A is injected in the internal electrodes while the external electrodes are passive. A negative sensibility means that an increase of the conductivity in this region will imply an increase of the measured impedance instead of a decrease of this impedance as it could be intuitively expected.

3. Results and discussion

3.1. In pulse DC electrical analysis

3.1.1. Real system simulations

In order to predict the impedance measured in our experiments, we performed a 3D simulation of the four-electrode system using the code described in Section 2.3.2 in the case of the conductivity model given by Eq. (4). An example of this calculation is given in Fig. 4 for an applied voltage between the external needles of 280 V; the average electric field $E_{average}$ defined as the ratio between the voltage applied between the external electrodes and the distance between those electrodes is 600 V/cm. Fig. 4a shows the electric field computed before the electroporation process starts: the distribution of the electric field is not uniform between the electrodes; the value of the electric field is approximatively 440 V/cm in the middle of the domain but it largely exceeds the average value of 600 V/cm in the vicinity of the electrodes. When the electroporation process is included in the model, Fig. 4b shows that an increase of the conductivity is observed in the vicinity of the external electrodes as well as near the internal electrodes corresponding to the stronger electric field induced in these regions. Finally, Fig. 4c shows the resulting electric field distribution when the change in conductivity produced by electroporation is considered. Notice how the electric field distribution considerably changes with respect to the initial situation.

In Fig. 4d the resulting sensitivity distribution computed from Eq. (8) is shown for the 4-electrodes geometry. The results are consistent with the 4-electrode device analyzed in [30]. The simulations show that there is a negative sensibility region between the external electrodes and the internal ones. It is precisely in this region where, according to Fig. 4b, there is a higher conductivity change (i.e. the area of higher electroporation). It is clear that in the present case, this could be a limitation for using this type of electrode arrangement in electroporation monitoring. Our model should automatically reflect this adverse effect since the electroporation process and the resulting impedance changes are simulated in the real geometry.

3.1.2. In vivo measurements

In order to make a mindful estimation of the variation in the intra-pulse tissue impedance during electroporation pulses in mice liver, voltage and current measurements were recorded before and during the pulses. As explained in Materials and Methods, two 100 μs pulses with a low electric field intensity under the threshold of electroporation were applied before the sequence of 8 electroporation pulses. From those pulses, the initial instantaneous tissue resistance $R_{pulse}(t)$ can be extracted as a reference. In Fig. 5a and b, an example of current and voltage recordings for three different applied voltages (280 V/$E_{average}$ = 600 V/cm, 460 V/$E_{average}$ = 1000-V/cm and 645 V/$E_{average}$ = 1400 V/cm) are shown. Notice how the actual values of the voltages acquired in the internal electrodes are lower than the values applied through the external electrodes. The corresponding dynamic evolution of the in-pulse resistance $R_{pulse}(t)$ normalized to the value of R_{pulse} (R_{pulse0}) at the beginning of the first pulse ($R_{norm} = R_{pulse}(t)/R_{pulse0}$) is shown in Fig. 5c. The recordings show a dynamic decrease of tissue resistance during the pulse application as a result of a progressive tissue permeabilization. The dynamics of this variation are dependent on the intensity of the applied electric field, with a more pronounced and faster change for the highest voltage applied. It is observed that the instantaneous resistance tends to a constant value at the end of each pulse and it seems that there is no cumulative impedance decrease over the whole pulse sequence contrary to other studies [8].

The values of the instantaneous resistance $R_{pulse}(t)$, calculated as the average of the voltage and current ratio at the end of each pulse (see Section 2.1.1), and its relative variation in percentage with respect to the initial state are shown in Table 1. Data shows the results for different electric field intensities applied in different animals (three different animals for electric field condition are shown). The relative drop in impedance increases with the intensity of the applied electric field with mean values (±standard devi-

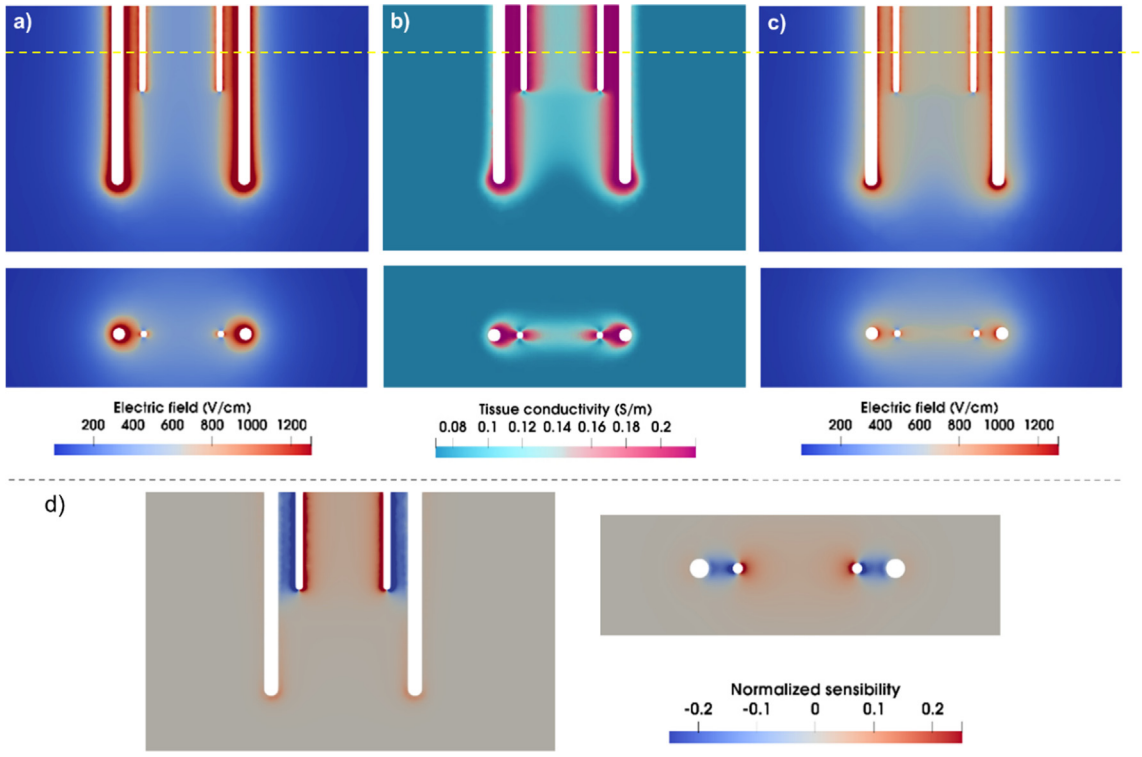

Fig. 4. Results of the 3D simulation of the four-electrode geometry in a parallel and perpendicular cut planes when 280 V are applied between the external electrodes (average electric field $E_{average}$ = 600 V/cm). (a) Distribution of the electric field if there were no effect of electroporation. (b) Distribution of the conductivity in the tissue using the nonlinear model of Eq. (4) when the applied voltage between the external needles is 280 V. The values introduced in Eq. (4) for the tissue conductivities are σ_{ext} = 0.07 S/m and σ_{int} = 0.15 S/m, respectively, as they were extracted from the analysis of the spectroscopy measurements performed before electroporation (see Supplementary Information I, part A). (c) Distribution of the electric field considering the effect of electroporation. (d) Distribution of the sensibility *S* in the 4-electrode system.

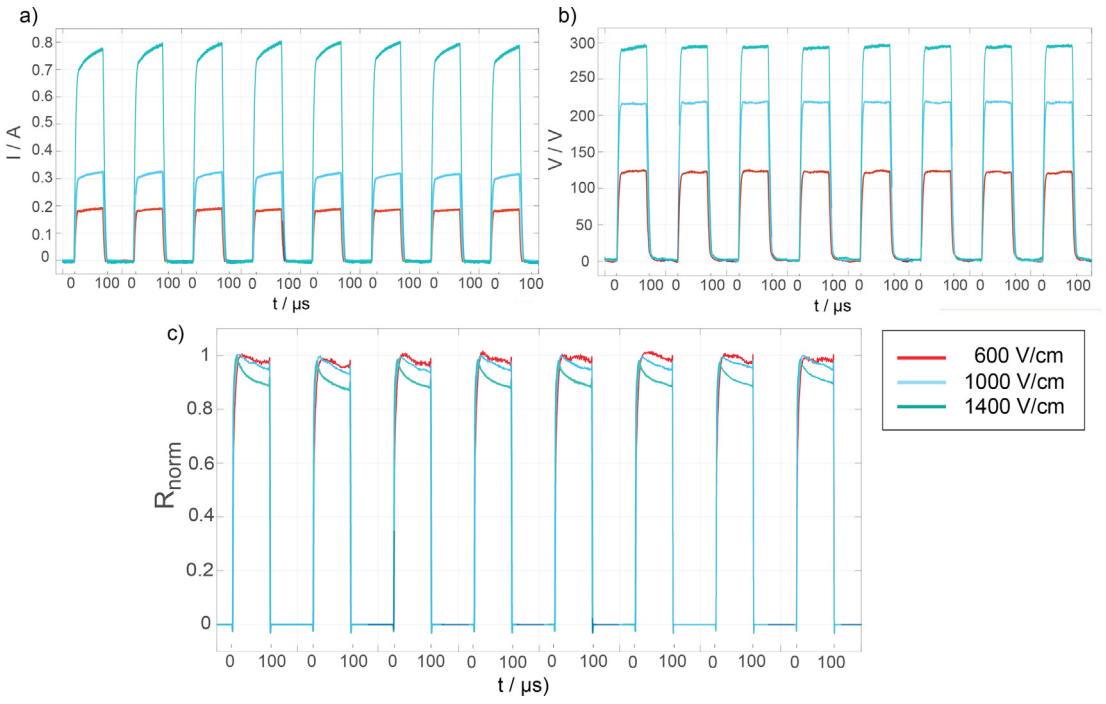

Fig. 5. (a) and (b) Examples of current and voltage recordings during electroporation for three different applied voltages (280 V, 460 V, and 645 V). (c) Calculated in-pulse resistance R_{pulse} for the corresponding examples in (a) and (b) normalized to the value at the beginning of the first pulse. The duration of each pulse was 100 µs and the sequence of 8 pulses was applied at a repetition frequency of 1 Hz. The horizontal axes are segmented to omit the space between pulses.

Table 1
instantaneous resistance $R_{pulse}(t)$ measured before and during the electroporation process. Percentage values correspond to the relative resistance drop with respect to the pre-electroporation state.

Applied voltage, Electric Field	Mouse number	Before	During
280 V, 600 V/cm	1	653 ± 17 Ω	550 ± 5 Ω/−16%
	2	789 ± 14 Ω	654 ± 5 Ω/−17%
	3	591 ± 9 Ω	478 ± 8 Ω/−19%
460 V, 1000 V/cm	4	940 ± 26 Ω	680 ± 7 Ω/−28%
	5	632 ± 10 Ω	478 ± 4 Ω/−24%
	6	799 ± 9 Ω	568 ± 2 Ω/−29%
645 V, 1400 V/cm	7	698 ± 11 Ω	417 ± 4 Ω/−40%
	8	546 ± 8 Ω	364 ± 6 Ω/−33%
	9	494 ± 7 Ω	317 ± 3 Ω/−36%

ation) of 18 ± 1.7%, 26.6 ± 2.3% and 35.3 ± 4.5% for 280 V, 460 V and 645 V, respectively.

Following, the mathematical model of Eq. (4) was used to compute the numerical values of the instantaneous resistance for the 4-electrodes system at the end of the pulse for a wide range of electric fields from 300 to 1500 V/cm. Additionally, the ideal case, which would be the measured resistance between two parallel plate electrodes of infinite extent, where the electric field is supposed to be constant, is shown for comparison. In these ideal conditions, $R_{pulse} = K/\sigma_{eq}$ where K is the form factor of two parallel plate electrodes system and, of course, it follows the sigmoid function previously described. Fig. 6a shows a comparison between the measurements and the computed values.

It is worth noting that the resistance computed by the model in the real 4-electrode geometry increases for electric field values between 300 and 500 V/cm contrarily to the ideal case. This result is due to the non-homogenous distribution of the electric field and the sensitivity considerations discussed in Section 3.1.1. The electric field in the vicinity of the electrodes is higher than the effective electric field at the center of the domain, which can cause electroporation only around the electrodes. However, the sensitivity S is negative precisely in that region; as a result, an increase of the conductivity will lead to an increase of the global impedance as calculated by the model. Subsequently, when the electric field exceeds the threshold for electroporation, there is a large drop of the resistance. Note that the threshold is 650 V/cm in the ideal case, which corresponds to the value of the parameter a of the conductivity model given in Eq. (4). For the 4-electrodes system, the threshold appears for a larger value of the average electric field: one has to keep in mind that the electric field is not uniform inside the tissue (the electric field given in the horizontal axis of Fig. 6 is the average electric field $E_{average}$ previously defined).

Fig. 6a shows a good agreement between the simulated results using Eq. (4) and the experimental results for an applied electric field of 600 V/cm but not for 1000 and 1400 V/cm: the decrease of the resistance is lower in the measurements compared to the simulated results. One reason for this disagreement could be the negative sensitivity areas around the external electrodes. As shown for the lowest electric field values, the model is able to capture this effect and the large difference between measurements and simulations (20–30%) could be attributed to a large increase of the local conductivity in the regions of negative sensitivity. Another possible reason for this disagreement is that the previous simulations were performed without taking into account the possible temperature effects due to the application of high intensity electric field pulses. As it was previously shown in other studies involving needles, temperature effects at the top and around the edge of the needles can be substantial [31]: a high temperature increase can involve a considerable increase of the tissue conductivity. In our particular

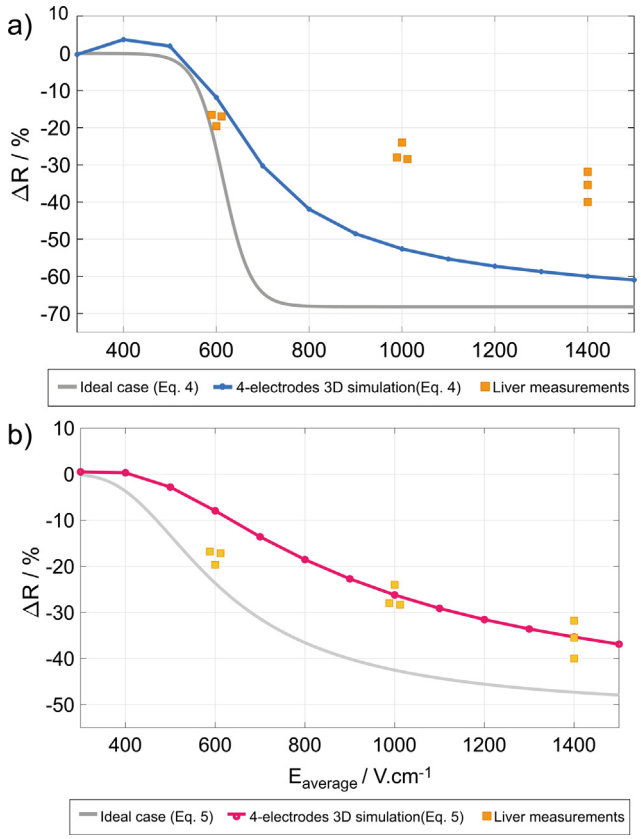

Fig. 6. Variation of the simulated equivalent resistance R_{eq} for the 4-electrodes system. The liver measurements correspond to the measured experimental resistance R_{pulse} at the end of the pulse (data from Table 1, three different animal per field condition). Additionally, the ideal case corresponding to the resistance between two parallel plates of infinite extent is shown for comparison. (a) The non-linear model for the tissue conductivity given by Eq. (4) is used in the simulation (a = 650 V/cm and b = 30 V/cm). (b) The electroporation model for the conductivity given by Eq. (5) is used in simulations (a′ = 800 V/cm). In both models, σ_{ext} = 0.07 S/m and σ_{int} = 0.15 S/m.

setup, this change in temperature/conductivity would be maximum in the regions of negative sensitivity.

Simulations with the model of Eqs. (6)–(7) have been performed with α_T = 1.5%/°C, ρ = 1000 kg/m^3, c_p = 3750 J/kg K which are the values commonly used for liver tissues in literature [32]; Δt = 800 μs according to the cumulative duration of the electric field application. Our simulations show an increase of temperature, confined to the vicinity of the external electrodes, of 0.6 °C, 3 °C and 7 °C for the average electric field of 600 V/cm, 1000 and 1400 V/cm, respectively. This temperature increase has nearly no effect on the equivalent resistance R_{eq} of the tissue. The simulations show that the variation of R_{eq} between the conductivity models $\sigma_{eq}(E)$ and $\sigma_{eq}(E, \Delta T)$ is 0.2%, 0.5% and 0.6% for values of the average electric field of 600 V/cm, 1000 and 1400 V/cm, respectively.

Finally, with the aim at providing numerical results in better agreement with the experimental results, simulations were performed with the model provided by Eq. (5). Using a suitable value for the parameter a'= 800 V/cm, Fig. 6b shows that this model provides numerical results closer to the experimental results compared to the model built with Eq. (4) what suggests that this function could better describe the present experimental situation. Nevertheless, as it will be shown below, other physiological changes during the electroporation process that modify the electrical properties of the extracellular medium could help to explain the observed disagreement between the simulations and the measurements.

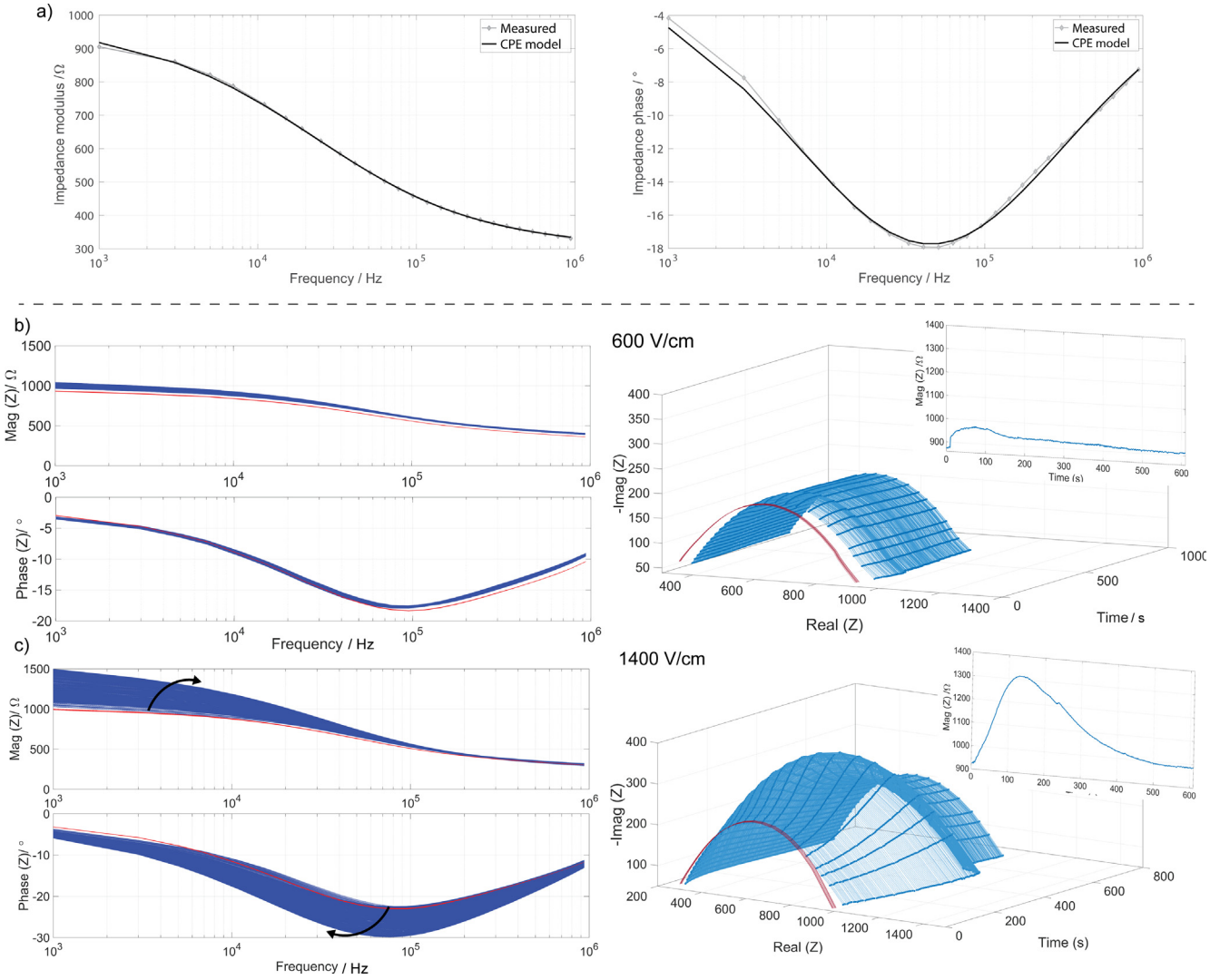

Fig. 7. Impedance spectroscopy measurements on liver tissue. (a) Example of preelectroporation impedance spectra (magnitude and phase) and the corresponding fitted CPE model for a mouse liver. Numerical results were obtained with R_{ext} = 978 Ω, R_{int} = 434 Ω, α = 0.64 and β = 4.4 10−7SI. (b) and (c) Example of impedance spectra evolution: before (red) and during 10 min immediately after electroporation pulses (blue) for an applied voltage of: b) 280 V ($E_{average}$ = 600 V/cm) and (c) 645 V ($E_{average}$ = 1400 V/cm). On the left, magnitude and phase evolution are shown. On the right, the corresponding Nyquist plots and detailed view of the temporal evolution of impedance magnitude at 5 kHz. (For interpretation of the references to colour in this figure legend, the reader is referred to the web version of this article.)

These results could have important implications in the design of the feedback control systems for the pulse generators used in the clinical practice. A pulse generator able to assess in real time the extent of tissue electroporation based on conductivity measurements could have enormous advantages [3]. Currently, the clinical systems enable visualizing the voltage and current traces but do not provide a real-time estimator of tissue electroporation. For that purpose, understanding what is the correct model to use and how the electrode geometry can impact the measurements is of outmost importance.

3.2. Electrical impedance spectroscopy measurements

In this section, the electrical impedance spectra from 1 kHz to 1 MHz measured in the liver tissue immediately before and during 10 min after electroporation pulses application are shown.

The impedance magnitude and phase spectra (uncalibrated) corresponding to the pre-electroporation state of one illustrative mouse liver are displayed in Fig. 7a. The measurements display the classical shape of an electrical impedance spectrum of biological tissues in the β dispersion range. Namely, a relaxation in the magnitude of the impedance is observed with increasing frequency due to the presence of insulating cell membranes. Additionally, a minimum in the phase corresponding with a pseudo capacitive behavior of cell membranes is also displayed. Notice how thanks to the 4-electrode measuring approach, the undesired effects at low frequency due to interfacial polarization of the electrodes are negligible: a relatively flat spectrum with a phase angle value close to zero is observed in the low frequency range. The observed behavior perfectly matches with the model previously presented in Section 2.3.1 (see Fig. 2) where the resistance R_m is neglected. Fig. 7a shows the simulated impedance spectra using the CPE model after identification of the parameters to minimize the distance between the experimental data and the simulation. A good agreement is obtained with values of R_{ext} = 978 Ω, R_{int} = 434 Ω, and β = 4.4 10^{-7}SI. The obtained value for α = 0.64 reveals a large dispersion of the relaxation times related to the interfacial polarization of cell membranes. From these measurements, the values for R_{int} and $R_{ext,}$ can be exploited further to extract the equivalent conductivity of the intra and extra cellular media before electroporation (see Supplementary Information I, part A).

Fig. 7b and c display the impedance spectra evolution during the 10 min immediately after pulse application for a representative example of the recordings performed either at 280 V ($E_{average}$ = 600-V/cm) and 645 V ($E_{average}$ = 1400 V/cm), , respectively (at least 3 repetitions for electric field were performed). The impedance spectrum $Z_{spectroscopy}(\omega)$ was recorded every second during 10 min. Both magnitude and phase evolution and the corresponding Nyquist plots are shown. In all cases, the impedance increased immediately after the pulses in the low frequency range while it remained nearly constant in the range of high frequencies. This observation does not follow the expected behavior where the impedance of an electroporated tissue should be lower immediately after pulse application as previously shown in [8]. Depending on the intensity of the electric field applied, the observed evolution of the impedance during the 10 min following pulse application was different.

In Fig. 8, the normalized mean (±SD) evolution of the low frequency impedance at 5 kHz for 600, 1000, 1400 and 1800 V/cm is shown for at least three different animals per group. In the case of the lowest electric field, the impedance at low frequency increased during the first minute and then decreased back to its initial value (see inserts on the right part of Fig. 7). Differently, for 1000 and 1400 V/cm, the increase of the impedance reached a maximum between 2 and 3 min after pulse application with a relative increase significantly higher than in the previous case and then it declined back to a value higher than its initial state. The large standard deviation observed for 1400 V/cm results from the fact that in some cases impedance recovered with similar dynamics than for 1000 V/cm while in other animals, the impedance recovery was much slower. Interestingly, the observed evolution for the highest electric field of 1800 V/cm displays a significantly lower maximum increase of impedance and the recovery of impedance back to the initial state was extremely slow or not noticeable for some animals. These observations will be discussed in detail in the next section.

Overall, the observed impedance evolution is very similar to the results shown by [8] in rat liver for the minutes after the electroporation application. However, in the mentioned study and contrary to the present results, the values of impedance immediately after pulse application were lower than the initial pre-electroporation values in agreement with an increased membrane conductivity immediately following electroporation. Also in that study, the measurements during and between pulses showed a continuous increase of conductivity (decrease of impedance) during the pulse sequence application. There could be several reasons to explain these differences:

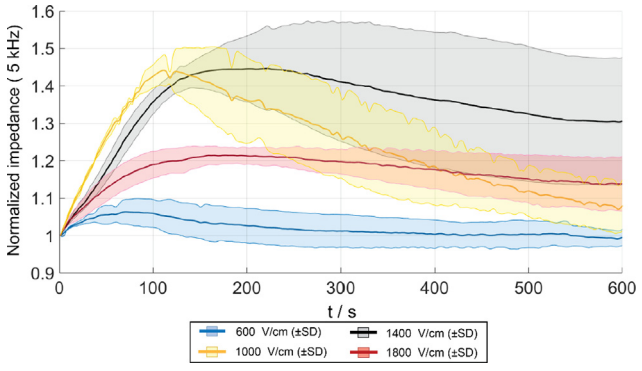

Fig. 8. Mean evolution (±SD) of impedance magnitude at 5 kHz normalized to the pre-electroporation values for different electric field intensities during 10 min after electroporation treatment. At least three animals per group were included to calculate the average values shown.

(i) An important difference is the geometry of the electrodes. The device proposed in [8] induces a more uniform electric field compared to our 4-electrodes system. In those conditions, the electroporation effects are expected to be closer to the ideal case. There are also differences in the sensitivity of the device: the system proposed in [8] induces much less negative sensitivity areas. However, the increase of the impedance for the spectroscopy measurements reported here cannot be fully explained by the areas of negative sensitivity of the system as discussed in Section 3.1 1.

(ii) In [8], the pulses were applied with a separation of 100 ms instead of 1 s in our case. The cumulative change in the tissue pulse after pulse will also be different from the present experimental conditions

(iii) Finally, another important difference concerns the portion of tissue treated. In our case, the size of the 4-electrodes system is comparable to the size of the liver lobe treated; in [8], a smaller portion of the rat liver is treated with the 4-electrodes system. If we make the assumption that physiological changes can greatly affect the electrical properties of the tissue, these changes will have a greater impact in our study.

In the next section, a theoretical analysis of the impact of the physiological changes is provided.

3.3. Theoretical analysis of the impact of macroscopic tissue changes in the electrical impedance of tissue after electroporation

In order to further analyze the observed increase in impedance, the mathematical model of the tissue proposed in Fig. 2 is considered. The resistance R_m is not considered here for different reasons:

(i) Spectroscopy data was recorded before and after the pulses application: molecular dynamics simulations predict that the pores are expected to appear only during the pulse and to disappear immediately after the electric field is turned off [35]. Consequently, although the state of permeabilization can last several minutes after the pulse onset, the state of high membrane conductivity ceases immediately after the pulse.

(ii) The membrane conductivity depends on the applied electric field because it is related to an electrodiffusion phenomenon [36]: the larger the transmembrane voltage is, the larger the conductivity of the membrane is. Since the electric field applied in spectroscopy analysis is very small compared to the one applied during the pulse (current intensity < 1 mA, see Section 2.1.2 for spectroscopy and between 0.2 and 0.8 A during the high electric field application, see Fig. 5); the membrane conductivity should be very small with a value of R_m comparable to the one in normal conditions (open circuit approximation).

(iii) A strong decrease of the tissue conductivity just at the end of the pulse has already been reported in other studies (see Figs. 4 and 5 in [8])

Neglecting R_m in the model of Fig. 2, the impedance in the low frequency range (called R_0) corresponds to the value of R_{ext}while the impedance in the high frequency range (called R_∞) corresponds to the parallel association of $R_{int}//R_{ext}$.

The values of R_{int} and R_{ext} extracted from the measurements have been used to calculate the evolution of R_0 and R_∞ during the 10 min after electroporation for the different electric fields studied (see Supplementary Information I, Fig. B1). The results for R_0 display a similar evolution than the low frequency impedance magnitude shown in the previous section. This evolution indicates that for large electric fields, there is a decrease of the

equivalent conductivity σ_{ext} of the extra cellular medium just after the pulses ($R_0 = K/\sigma_{ext}$). On the opposite for R_∞, the values are nearly constant during the whole acquisition time for the four cases analyzed: the variation does not exceed a few percent. This means that the equivalent conductivity σ_∞ ($=\sigma_{int} + \sigma_{ext}$) of the tissue remains nearly constant ($R_\infty = K/\sigma_\infty$).

These observations can be explained by changes in the intracellular volume. Using mixture formula (see Supplementary Information I, part C), the volume fraction f of the intracellular medium can be computed from the value of the resistance R_0 and R_∞ as follows:

$$f = 2 \times \frac{R_0 - R_\infty}{2R_0 + R_\infty} \tag{9}$$

3.4. Correlation of the impedance changes and the vascular lock effect

Following the theoretical explanation given in the previous section, the evolution of the volume fraction of the extracellular medium after electroporation was calculated for the different values of the electric field studied using Eq. (9). Subsequently, the temporal evolution of the calculated fraction of extra cellular volume (1 − f) was fitted to a lognormal law expressed by:

$$1 - f(t) = \left(1 - f_{|t=0}\right)\left(1 - M\frac{exp\left[-(ln(t) - \mu)^2/(2\sigma^2)\right]}{t\sigma\sqrt{2\pi}}\right) \tag{10}$$

From this equation, the identification for the parameters {M, μ, σ} was performed in order to minimize the distance between the lognormal model and the estimated value f obtained from the mixture formula for the whole impedance recording duration. Fig. 9 shows the calculated values and the fitted lognormal curve displaying the good agreement between measurements and the model for 1000 V/cm, 1400 V/cm and 1800 V/cm. For 600 V/cm the variation of the computed volume fraction is very small, almost negligible. However, for 1000 V/cm and 1400 V/cm, there is a fast decrease of the extracellular medium volume between + 15% and + 18% during the first 2–3 min; then, the fraction of extracellular medium increases slowly during 8 min. In the case of 1000 V/cm the recovery to the initial values is almost complete, on the contrary for 1400 V/cm, the recovery was variable: in some animals the recovery dynamics were slow while in other cases the recovery was almost complete in the 10 min recording time. Finally, for the highest electric field the variation observed in this parameter was considerably lower than in the previous exposure conditions. This observation suggests that for 1800 V/cm there are changes in the tissue that could mask or dominate the changes in the tissue volume fraction.

Among the possible phenomena explaining the measured change in volume fraction between the intracellular and extracellular spaces, there are two more likely events in the case of an electroporated tissue: these are cell swelling and/or the modification in the tissue vasculature in the electroporated region. The first would lead to an increase in the intracellular volume (and a reduction in the extracellular space) due to the influx of water through the permeabilized cell membranes to reduce the osmotic imbalance produced by the transport of ions and small molecules. If this effect were dominant, the significant changes in the ions concentration and water content would lead to changes in the local conductivities of both the intracellular and extracellular spaces of the tissue, which, according to the previous section, cannot explain the observed impedance evolution. Additionally, although this effect has been observed in vitro, no evidence of it has been provided in vivo.

On the contrary, the changes in the vasculature after electric pulses application have been widely observed in vivo in tumors, liver, and muscle [37–39]. In the particular case of liver, Ramirez et al. confirmed the absence of blood flow immediately after reversible electroporation pulse application in rabbits [38]. This early effect has been explained as the local occlusion of the afferent vasculature to the tissue and is known as “vascular lock”. This early effect has a limited duration (5–10 min) and is fully reversible. The most plausible explanation that is usually attributed to this observation is the reflexory vasoconstriction of afferent arterioles mediated by the sympathetic nervous system [37]. A reduction in the diameters of all affected blood vessels has been observed in different studies [40,41] with a predominant vasoconstriction in arterioles and in a lesser extend in venules [41], probably due to the smooth muscle cells layer present on them. A second and delayed effect in the vasculature after electroporation is an increased state of permeabilization of blood vessels that leads to a leaky state up to 30 min post electroporation. Vascular effects after electroporation are considered beneficial to avoid bleeding or to retain a drug in the tumor site for a longer time. These two phenomena combined can explain a change in the intracellular/extracellular volume fraction not caused by an increase in the intracellular space (cell swelling) but on the contrary by a decrease of the extracellular volume. The highly conductive extracellular fluid content would be reduced by the stop in the blood supply from the afferent system while the venous system, although leaky, could still recover the blood from the tissue due to the lower vasoconstriction observed and the negative pressure of the venous circulatory system. This way, the extracellular space of the tissue would temporarily “dehydrate” leading to an increase in the electrical impedance in accordance to our measurements. The above explanation leads us to conclude that the dynamics of blood vessels occlusion and reopening control the evolution of the tissue impedance after electroporation. This match between the amount of blood arriving to the tissue and impedance has been previously proposed during ischemia in myocardial tissue [42,43] or in liver [44]. This interpretation also explains why at the highest electric field condition, where extensive and likely irreversible permeabilization occurs, the changes in the ratio between intracellular and extracellular spaces are affecting less to the impedance measurements because cell membrane integrity is compromised.

Interestingly, a recent study about the vascular effects induced by electroporation performed by Golzio et al. fully supports our interpretation. In [40] authors report experimental results where electroporation induced diameter variations of the vessels in a similar way to our impedance measurements. More significantly, the study is detailed in Pefoly’s thesis [45] where the time evolution of the vessel diameters is fitted with a type (1-lognormal) law:

$$d(t) = d_{|t=0} \times \left(1 - M\frac{exp\left[-(ln(t) - \mu)^2/(2\sigma^2)\right]}{t\sigma\sqrt{2\pi}}\right) \tag{11}$$

In [45], M varies in the range {90, 350} depending on the nature of the vessels (arteriole, small or large venules) while μ is found to be in a small range {5.15, 5.44} as well as σ {1.08, 1.25}. The values of the parameters for the lognormal law μ and σ are in the same range of values that the ones found in our study. Since those parameters define the temporal dynamics of vessel constriction and opening, one could conclude that probably a similar phenomenon is involved in both experiments.

The link shown between the impedance evolution and the vascular effects in the electroporated liver demonstrates that the interpretation of impedance measurements after the pulse application to assess the success of a treatment is not straightforward. From a clinical perspective, where a system based on impedance measurements could be a way to have information about the extent and level of tissue electroporation, we demonstrate here that developed models should take into consideration other complex phenomena taking place in parallel to electroporation.

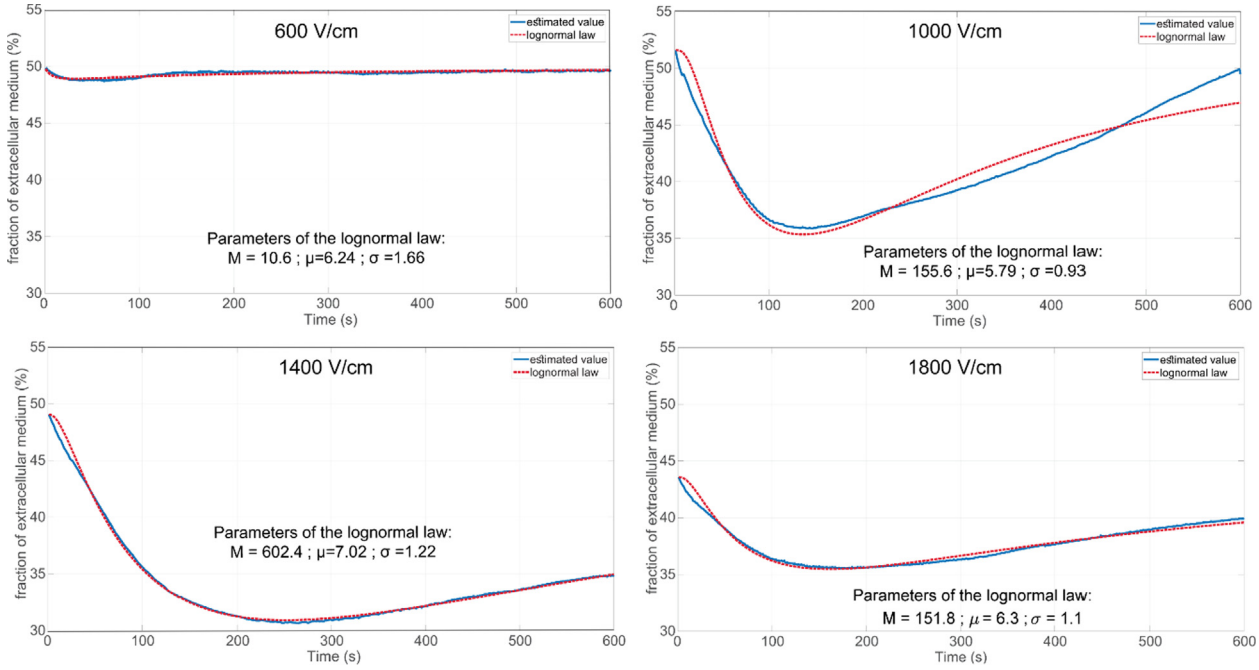

Fig. 9. Evolution of the fraction of the extra cellular volume after the application of the pulses for the different applied electric fields.

4. Conclusions

Impedance measurements have been performed using a 4-electrode system where needles were inserted inside a liver tissue in order to monitor in vivo the state of the tissue throughout the electroporation process. The data recorded before, during and after the pulses were used to perform numerical simulations based on a traditional model. We found that the standard numerical models do not provide consistent results, which proves that collateral phenomena that are not generally taken into account are at work during the process of electroporation in vivo. It appeared in our experiences that a vascular lock significantly modifies the volume of the intra and extra cellular media, which changes dramatically the electrical properties of the tissue. The dynamics of this vascular lock has been studied and coincide with the data presented by Golzio's group on the contraction of blood vessels after the pulses application.

Compared to other studies reported in literature, the physiological effects that we observed were amplified due to the experimental configuration where the size of the 4-electrode system is not small compared with the size of the biological organ. Nevertheless, these effects are present, probably in a lesser extent, in other experiments reported by other groups. One serious issue is to quantify the consequences of physiological effects in the analysis of impedance measurement performed during the pulses and separate them from the effects of electroporation on cell membranes; indeed, the vascular lock can be initiated in the time interval during which the sequence of pulses is applied. The present results could have important implications in future clinical feedback control systems used to assess the success of an electroporation treatment.

Declaration of Competing Interest

The authors declare that they have no known competing financial interests or personal relationships that could have appeared to influence the work reported in this paper.

Acknowledgments

This work was partially funded by the ITMO Cancer in the frame of the Plan Cancer 2014–2019 (projects PC201515 and PC201615) and "La Ligue contre le Cancer" postdoctoral fellowship program. The authors thank the funding support of the CNRS, Gustave Roussy, Univ. Paris-Sud and Université Paris-Saclay. The authors declare no conflict of interest. DV and CP are grateful to Annabelle Collin, Assistant Professor at Bordeaux INP, for helpful discussions and advices on the implementation of the numerical method.

Ethical statement

All applicable international, national, and/or institutional guidelines for the care and use of animals were followed.

Appendix A. Supplementary material

Supplementary data to this article can be found online at https://doi.org/10.1016/j.bioelechem.2020.107627.

References

[1] K. Kinosita Jr, T.Y. Tsong, Voltage-induced conductance in human erythrocyte membranes, Biochim. Biophys. Acta - Biomembr. 554 (2) (1979) 479–497.
[2] M. Schmeer, T. Seipp, U. Pliquett, S. Kakorin, E. Neumann, Mechanism for the conductivity changes caused by membrane electroporation of CHO cell-pellets, PCCP 6 (24) (2004) 5564–5574.
[3] D. Cukjati, D. Batiuskaite, F. Andre, D. Miklavcic, L.M. Mir, Real time electroporation control for accurate and safe in vivo non-viral gene therapy, Bioelectrochemistry 70 (2) (2007) 501–507.
[4] T. Blagus et al., In vivo real-time monitoring system of electroporation mediated control of transdermal and topical drug delivery, J. Control. Release 172 (3) (2013) 862–871.
[5] R.M. Atkins et al., Impedance spectroscopy as an indicator for successful in vivo electric field mediated gene delivery in a murine model, Bioelectrochemistry 115 (2017) 33–40.
[6] Y. Zhao, H. Liu, S.P. Bhonsle, Y. Wang, R.V. Davalos, C. Yao, Ablation outcome of irreversible electroporation on potato monitored by impedance spectrum under multi-electrode system, Biomed. Eng. Online 17 (1) (2018) 1–13.

[7] D. Šel, D. Cukjati, D. Batiuskaite, T. Slivnik, L.M. Mir, D. Miklavčič, Sequential finite element model of tissue electropermeabilization, IEEE Trans. Biomed. Eng. 52 (5) (2005) 816–827.
[8] A. Ivorra, B. Rubinsky, In vivo electrical impedance measurements during and after electroporation of rat liver, Bioelectrochemistry 70 (2) (2007) 287–295.
[9] A. Silve, A. Guimerà Brunet, B. Al-Sakere, A. Ivorra, L.M. Mir, Comparison of the effects of the repetition rate between microsecond and nanosecond pulses: electropermeabilization-induced electro-desensitization?, Biochim. Biophys. Acta - Gen. Subj. 1840 (7) (2014) 2139–2151.
[10] T. García-Sánchez, I. Leray, M. Ronchetti, R. Cadossi, L.M. Mir, Impact of the number of electric pulses on cell electrochemotherapy in vitro: limits of linearity and saturation, Bioelectrochemistry 129 (2019) 218–227.
[11] B. Gabriel, J. Teissié, Control by electrical parameters of short- and long-term cell death resulting from electropermeabilization of Chinese hamster ovary cells, Biochim. Biophys. Acta - Mol. Cell Res. 1266 (2) (1995) 171–178.
[12] A. Ivorra, B. Al-Sakere, B. Rubinsky, L.M. Mir, In vivo electrical conductivity measurements during and after tumor electroporation: conductivity changes reflect the treatment outcome, Phys. Med. Biol. 54 (19) (2009) 5949–5963.
[13] T. García-Sánchez, R. Bragós, L.M. Mir, In vitro analysis of various cell lines responses to electroporative electric pulses by means of electrical impedance spectroscopy, Biosens. Bioelectron. 117 (2018) 207–216.
[14] Q. Castellví, B. Mercadal, A. Ivorra, Assessment of Electroporation by Electrical Impedance Methods, in: D. Miklavčič (Ed.), Handbook of Electroporation, Springer International Publishing, Cham, 2017, pp. 671–690.
[15] E.T. McAdams, A. Lackermeier, J.A. McLaughlin, D. Macken, J. Jossinet, The linear and non-linear electrical properties of the electrode-electrolyte interface, Biosens. Bioelectron. 10 (1–2) (1995) 67–74.
[16] D.E. Chafai, A. Mehle, A. Tilmatine, B. Maouche, D. Miklavčič, Assessment of the electrochemical effects of pulsed electric fields in a biological cell suspension, Bioelectrochemistry 106 (2015) 249–257.
[17] S. Rush, J.A. Abildskov, R. Mcfee, Resistivity of body tissues at low frequencies, Circ. Res. 12 (1) (1963) 40–50.
[18] Y. Wang, P.H. Schimpf, D.R. Haynor, Y. Kim, Geometric effects on resistivity measurements with four-electrode probes in isotropic and anisotropic tissues, IEEE Trans. Biomed. Eng. 45 (7) (1998) 877–884.
[19] U. Pliquett, R. Elez, A. Piiper, E. Neumann, Electroporation of subcutaneous mouse tumors by rectangular and trapezium high voltage pulses, Bioelectrochemistry 62 (1) (2004) 83–93.
[20] R.E. Neal et al., In vivo irreversible electroporation kidney ablation: experimentally correlated numerical models, IEEE Trans. Biomed. Eng. 62 (2) (2015) 561–569.
[21] D. Voyer, A. Silve, L.M. Mir, R. Scorretti, C. Poignard, Dynamical modeling of tissue electroporation, Bioelectrochemistry 119 (2018) 98–110.
[22] L.F. Cima, L.M. Mir, Macroscopic characterization of cell electroporation in biological tissue based on electrical measurements, Appl. Phys. Lett. 85 (19) (2004) 4520–4522.
[23] R.E. Neal, P.A. Garcia, J.L. Robertson, R.V. Davalos, Experimental characterization and numerical modeling of tissue electrical conductivity during pulsed electric fields for irreversible electroporation treatment planning, IEEE Trans. Biomed. Eng. 59 (4) (2012) 1076–1085.
[24] D.R. Cantrell, S. Inayat, A. Taflove, R.S. Ruoff, J.B. Troy, Incorporation of the electrode-electrolyte interface into finite-element models of metal microelectrodes, J. Neural Eng. 5 (1) (2008) 54–67.
[25] T. García-Sánchez, A. Azan, I. Leray, J. Rosell-Ferrer, R. Bragós, L.M. Mir, Interpulse multifrequency electrical impedance measurements during electroporation of adherent differentiated myotubes, Bioelectrochemistry 105 (2015).
[26] D. Miklavčič, N. Pavšelj, F.X. Hart, Electric properties of tissues, Wiley Encyclopedia of Biomedical Engineering, 2006.
[27] S.G. and O.G. Martinsen, Bioimpedance and Bioelectricity Basics. Academic Press, San Diego, CA, 2000.
[28] C. Geuzaine, J.-F. Remacle, Gmsh: a 3-D finite element mesh generator with built-in pre- and post-processing facilities, Int. J. Numer. Meth. Eng. 79 (11) (2009) 1309–1331.
[29] M. Breton et al., Non-linear steady-state electrical current modeling for the electropermeabilization of biological tissue, IEEE Trans. Magn. 51 (3) (2015) 3–6.
[30] F. Hecht, New development in FreeFem++, J. Numer. Math. 20 (3–4) (2012) 251–266.
[31] R.V. Davalos, B. Rubinsky, L.M. Mir, Theoretical analysis of the thermal effects during in vivo tissue electroporation, Bioelectrochemistry 61 (1–2) (2003) 99–107.
[32] P.A. Garcia, J.H. Rossmeisl, R.E. Neal, T.L. Ellis, R.V. Davalos, A parametric study delineating irreversible electroporation from thermal damage based on a minimally invasive intracranial procedure, Biomed. Eng. Online 10 (1) (2011) 34.
[33] G. Sverre, G.M. Ørjan, Sources of error in tetrapolar impedance measurements on biomaterials and other ionic conductors, J. Phys. D Appl. Phys. 40 (1) (2007) 9.
[34] W. Van Den Bos et al., Thermal energy during irreversible electroporation and the influence of different ablation parameters, J. Vasc. Interv. Radiol. 27 (3) (2016) 433–443.
[35] M. Tarek, Membrane electroporation: a molecular dynamics simulation, Biophys. J. 88 (6) (2005) 4045–4053.
[36] K.A. DeBruin, W. Krassowska, Modeling electroporation in a single cell. II. Effects of ionic concentrations, Biophys. J. 77 (3) (1999) 1225–1233.
[37] G. Serša, M. Cemažar, B. Markelc, Blood flow modifying and vascular-disrupting effects of electroporation and electrochemotherapy, Handbook of Electroporation, 2017.
[38] L.H. Ramirez' et al., Electrochemotherapy on liver tumours in rabbits, 1998.
[39] J. Gehl, T. Skovsgaard, L.M. Mir, Vascular reactions to in vivo electroporation: characterization and consequences for drug and gene delivery, Biochim. Biophys. Acta - Gen. Subj. 1569 (1–3) (2002) 51–58.
[40] E. Bellard et al., Intravital microscopy at the single vessel level brings new insights of vascular modification mechanisms induced by electropermeabilization, J. Control. Release 163 (3) (2012) 396–403.
[41] B. Markelc et al., In vivo molecular imaging and histological analysis of changes induced by electric pulses used for plasmid dna electrotransfer to the skin: a study in a dorsal window chamber in mice, J. Membr. Biol. 245 (9) (2012) 545–554.
[42] R. Bragos, P.J. Riu, M. Warren, M. Tresanchez, A. Carreno, J. Cinca, Changes in myocardial impedance spectrum during acute ischemia in the in-situ pig heart, Annu. Int. Conf. IEEE Eng. Med. Biol. - Proc. 5 (1996) 1953–1954.
[43] E. Jorge, G. Amorós-Figueras, T. García-Sánchez, R. Bragós, J. Rosell-Ferrer, J. Cinca, Early detection of acute transmural myocardial ischemia by the phasic systolic-diastolic changes of local tissue electrical impedance, Am. J. Physiol. Heart Circ. Physiol. 310 (3) (2016).
[44] D. Haemmerich et al., Changes in electrical resistivity of swine liver after occlusion and postmortem, Med. Biol. Eng. Comput. (2002).
[45] S. Pefoly, Applications thérapeutiques de l'électroperméabilisation en cancérologie, 2013.